THE JOURNAL OF BIOLOGICAL CHEMISTRY VOL. 285, NO. 4, pp. 2771–2782, January 22, 2010
© 2010 by The American Society for Biochemistry and Molecular Biology, Inc. Printed in the U.S.A.

Constitutive Activity of the Human TRPML2 Channel Induces Cell Degeneration*[S]

Received for publication, July 21, 2009, and in revised form, November 19, 2009 Published, JBC Papers in Press, November 23, 2009, DOI 10.1074/jbc.M109.046508

Shaya Lev[‡], David A. Zeevi[§], Ayala Frumkin[§], Vered Offen-Glasner[§], Gideon Bach[§], and Baruch Minke[‡1]

From the [‡]Department of Medical Neurobiology and the Kühne Minerva Center for Studies of Visual Transduction, Faculty of Medicine of the Hebrew University, and the [§]Department of Human Genetics, Hadassah Hebrew University Hospital, Jerusalem 91120, Israel

The mucolipin (TRPML) ion channel proteins represent a distinct subfamily of channel proteins within the transient receptor potential (TRP) superfamily of cation channels. Mucolipin 1, 2, and 3 (TRPML1, -2, and -3, respectively) are channel proteins that share high sequence homology with each other and homology in the transmembrane domain with other TRPs. Mutations in the TRPML1 protein are implicated in mucolipidosis type IV, whereas mutations in TRPML3 are found in the *varitint-waddler* mouse. The properties of the wild type TRPML2 channel are not well known. Here we show functional expression of the wild type human TRPML2 channel (h-TRPML2). The channel is functional at the plasma membrane and characterized by a significant inward rectification similar to other constitutively active TRPML mutant isoforms. The h-TRPML2 channel displays nonselective cation permeability, which is Ca^{2+}-permeable and inhibited by low extracytosolic pH but not Ca^{2+} regulated. In addition, constitutively active h-TRPML2 leads to cell death by causing Ca^{2+} overload. Furthermore, we demonstrate by functional mutation analysis that h-TRPML2 shares similar characteristics and structural similarities with other TRPML channels that regulate the channel in a similar manner. Hence, in addition to overall structure, all three TRPML channels also share common modes of regulation.

The mucolipin (TRPML) proteins represent a distinct subfamily of channel proteins within the transient receptor potential (TRP)[2] superfamily of cation channels (1). TRP channels are essential components of biological sensors that detect changes in the environment in response to a myriad of stimuli including cold or hot temperatures, natural chemical compounds, and mechanical stimuli. They participate crucially in many sensory modalities (2, 3). TRP channel proteins are found in a variety of organisms, tissues, and cell types including excitable and non-excitable cells and comprise an evolutionarily conserved non-specific cation channel family consisting of nearly 30 human members (1). The founding member of this family was discovered in *Drosophila* and was designated TRP by Minke *et al.* (4). The TRP superfamily is divided into seven subfamilies, one being the mucolipin-TRPML subfamily. Mucolipin 1, 2, and 3 (TRPML1, -2, and -3, respectively) are channel proteins that share high sequence homology with each other and homology in the transmembrane domain with other TRPs. Transmembrane segments 5 and 6 represent the predicted cation channel pore of these proteins (5, 6), as is true for all other TRP channels. Although most other TRPs localize and function primarily at the cell surface (3, 7, 8) mediating cell-environment interactions, TRPMLs and primarily TRPML1 are distinct in their lysosomal subcellular localization (9). TRPML1 displays strict lysosomal localization, whereas TRPML2 and -3 display cell surface as well as endosomal and lysosomal localization (9–15). Biochemical interactions have also been observed between TRPML1, -2, and -3 in homo- and heteromultimeric combinations (9, 15, 16). Multimeric interactions, in general, have been well documented in the TRP superfamily among protein members of the same subfamily (17) and also between subfamilies (18) (for review, see Ref. 19). It is also documented that TRPML1, -2, and -3 are expressed in many different tissues and cell types including brain tissue (20–22).

Loss of function mutations in the TRPML1 protein are implicated in mucolipidosis type IV (MLIV; MIM 252650), an autosomal recessive neurodegenerative disorder found with increased frequency in the Ashkenazi Jewish population, and characterized by motor impairment, mental retardation, and retinal degeneration (6, 23, 24). MLIV is characterized as a lysosomal storage disorder whereby lipids accumulate together with water-soluble materials in the lysosomes of cells from every tissue and organ of MLIV patients (25). Although the etiology of the disease and the role of TRPML1 role in causing it are well documented, the physiological function of TRPML1 has not yet been fully elucidated. Electrophysiological studies involving TRPML1 have shown that it is a non-selective cation channel whose activity is modulated by pH and Ca^{2+} (26–28). However, the precise cation permeability of this channel protein has also been a subject of controversy in recent years (28–32).

To date TRPML2 has not been associated with any human pathology, and its physiological role and inherent properties are

* This work was supported, in whole or in part, by National Institutes of Health Grant RO1 EY 03529 (to B. M.). This work was also supported by the Israel Science Foundation (to B. M. and G. B.), the United States-Israel Binational Science Foundation (to B. M.), the Moscona Foundation (to B. M.), the Minerva Foundation (to B. M.), and the Rita Altura foundation (to G. B.).

[S] The on-line version of this article (available at http://www.jbc.org) contains supplemental Figs. 1 and 2.

[1] To whom correspondence should be addressed: Dept. of Medical Neurobiology, Faculty of Medicine, The Hebrew University, P. O. Box 12272, Jerusalem 91120, Israel. Fax: 972-2-6439736; E-mail: baruchm@ekmd.huji.ac.il.

[2] The abbreviations used are: TRP, transient receptor potential; TRPL, TRP-like; Arf6, ADP ribosylation factor 6; LA, linoleic acid; NMDG, *N*-methyl-D-glucamine; MLIV, mucolipidosis type IV; h-TRPML, human TRPML; PMCA2, plasma membrane calcium ATPase type 2; HEK cells, human embryonic kidney cells; TES, 2-{[2-hydroxy-1,1-bis(hydroxymethyl)ethyl]amino}ethanesulfonic acid; MES, 4-morpholineethanesulfonic acid; WT, wild type; EYFP, enhanced yellow fluorescent protein; EGFP, enhanced green fluorescent protein.

poorly understood. Nevertheless, an active role has been proposed for this protein in trafficking and regulation along the clathrin-independent Arf6-associated endocytic pathway (10). In addition, analysis of the Bruton's tyrosine kinase (*Btk*) pathway in a *Btk* mouse knock-out model has implicated TRPML2 in B-lymphocyte development (33, 34).

Like TRPML2, TRPML3 has not been associated with a human pathology to date. Nevertheless, TRPML3 missense mutations, A419P and I362T, have been identified in the *varitint-waddler* mouse mutant, characterized by pigmentation defects and hearing loss. Mice homozygous for the A419P (Va) missense mutation in TRPML3 are predominantly embryonic lethal, whereas viable mice of this genotype display hearing loss, circling behavior, and pigmentation defects (35). Recent studies have shown that this severe phenotype results from constitutive and enhanced activation of the TRPML3 ion channel, leading to apoptosis in affected cells where mouse melanocyte and hair cells have been shown to be particularly sensitive to the A419P gain-of-function variant of TRPML3. The TRPML3-A419P mutant channel displays a distinct inwardly rectifying current voltage relationship (I-V curve) that causes cell death by inducing cell Ca^{2+} overload (20, 28, 36–39). A milder phenotype is found in Va^{J} *varitint-waddler* mice, characterized by normal vestibular function, partial pigmentation deficiency, and partial hearing loss. These mice have been shown to express a second TRPML3 missense mutation, I362T, in *cis* to the severe A419P mutation (35, 40). When expressed alone, the I362T TRPML3 mutant has been shown to lack channel activity in a mammalian expression system; however, when expressed in *cis* with the A419P mutation, it has been suggested that I362T ameliorates the lethal effects of A419P by reducing cell surface expression of TRPML3 (20).

The electrophysiological properties of the human wild type TRPML3 channel (h-TRPML3) have been described by Kim *et al.* (20). It was found that TRPML3 is a Ca^{2+}-permeable channel that is regulated by extracytosolic pH and that the channel can be opened by reintroducing Na^{+} to an Na^{+}-depleted extracellular solution (20, 41). Other groups have also described the constitutively active A419P mutant form of the TRPML3 channel. The permeability properties of this channel seems to be a point of debate (20, 28, 29). In HEK cells, TRPML1 and TRPML2 are not constitutively active, and as of yet, there is no known activator of these channels, unlike the case for several other TRP channels (*e.g.* TRPM8 activation by menthol (42)). However, when the A419P mutation was introduced into paralogous sites in murine isoforms of TRPML1 and TRPML2, the open probability of murine TRPML1-V432P was greatly enhanced at negative membrane potentials, whereas both long TRPML2-A424P and short TRPML2-A396P murine isoforms were also constitutively active (21, 28, 29). Murine TRPML1-V432P and the short murine TRPML2-A396P mutant also feature the same I-V curve as TRPML3-A419P, with similar biophysical properties, including conductance to Ca^{2+}, which is the cause of cell degeneration observed in mice and cells heterologously expressing this mutated form of the channel (28, 29, 37). However, unlike murine TRPML3-A419P, murine TRPML1-V432P and TRPML2-A396P are also permeable to Fe^{2+}, indicating that some features differ between the channels (28, 29).

Unlike in mice, the human TRPML2 (h-TRPML2) channel is found solely in a single isoform whose electrophysiological properties are poorly understood. It is, thus, important to characterize the wild type properties of this channel and compare them to the properties of mutated channel isoforms.

To gain an improved understanding of the properties and characteristics of the h-TRPML2 channel, we sought to express the channel in S2 Schneider cells (S2) (a *Drosophila* cell line derived from an embryonic cell lineage (43)) where some TRP channels exhibit constitutive activity. It was previously found that the *Drosophila* light-activated TRP-like (TRPL) channels, which are closed in the dark in native photoreceptor cells, become constitutively active when expressed heterologously in S2 cells (44, 45). The advantage of using the *Drosophila* S2 cell expression system is that the small endogenous currents of S2 cells are well characterized, making their effect upon heterologously expressed channels negligible. Also, mammalian proteins in S2 cells might be subject to weaker regulation, allowing for their functional expression. Here we show functional expression of h-TRPML2 in S2 cells. The channel is functional at the plasma membrane and characterized by a significant inward rectification, similar to that reported for other TRPML mutant channels that are constitutively active (28). The h-TRPML2 channel displays non-selective cation permeability, which is pH- but not Ca^{2+}-regulated, and constitutive activity of h-TRPML2 leads to cell death by Ca^{2+} overload. Furthermore, functional mutation analysis reveals that h-TRPML2 shares similar characteristics and structural similarities with other TRPML channels that regulate the channel in a similar manner.

EXPERIMENTAL PROCEDURES

Expression Constructs—The complete EYFP open reading frame was derived from the pEYFP-N1 vector (Clontech) and cloned into a slightly modified version of pMT/V5-His B (Invitrogen). tdTomato nucleotide sequences with and without a stop codon were derived from the pRSET-B tdTomato bacterial expression construct, kindly provided by Dr. Roger Tsien (Dept. of Pharmacology, University of California, San Diego), and cloned into the same pMT/V5-His B vector. During subsequent cloning steps, the V5 and His tags on the pMT vector were eliminated from all expression constructs. The human TRPML3 open reading frame (GenBank™ accession no. NM_018298), derived from control human lymphoblastoid cells, was cloned downstream to and in-frame with the tdTomato sequence on the pMT-tdTomato vector. The resulting pMT-tdTomato-TRPML3 construct was then used to prepare the pMT-tdTomato-TRPML3-A419P construct. The human TRPML2 open reading frame minus a stop codon (GenBank™ accession no. NM_153259), derived from control human lymphoblastoid cells, was cloned upstream to and in-frame with EYFP and tdTomato sequences on the appropriate pMT-EYFP and pMT-tdTomato vectors, respectively. The resulting pMT-tdTomato-TRPML3-A419P, pMT-TRPML2-YFP, and pMT-TRPML2-tdTomato fusion protein constructs were each used for expression in Schneider 2 (S2) cells. All directed mutations

in TRPML3 and TRPML2 were introduced into the pMT-tdTomato-TRPML3 and the pMT-TRPML2-tdTomato constructs, respectively, by site-directed mutagenesis according to a previously described method (46). For expression in HEK cells, fusion protein constructs were subcloned into the pcDNA3 mammalian expression vector (Invitrogen). For each construct described above, insert orientation and polymerase fidelity were verified by restriction enzyme mapping and sequencing. The pEGFP-TRPML3 and PMCA2z/a constructs used in this study were kindly provided by Dr. Shmuel Muallem (University of Texas Southwestern Medical Center, Dallas, TX) and Dr. Peter G. Gillespie (Oregon Hearing Research Center, Portland, OR), respectively.

Cell Culture—Schneider S2 cells were grown in 25-cm^2 flasks at 25 °C in Schneider medium (Biological Industries, Beit Haemek, Israel) supplemented with 10% fetal bovine serum and 1% penicillin-streptomycin. S2 cells, stably expressing TRPL-EGFP (TRPL accession number NM_165694) channels, were obtained from Dr. Armin Huber (University of Hohenheim, Stuttgart, Germany). All TRPML constructs for expression in S2 cells were inserted into pMT vectors as described above and transiently expressed using the escort IV transfection reagent (Sigma).

Human embryonic kidney and HeLa cells were grown in 25-cm^2 flasks at 37 °C in Dulbecco's modified Eagle's medium (Biological Industries) supplemented with 10% fetal bovine serum, 1% penicillin-streptomycin, and 1% L-glutamine. All TRPML constructs for expression in mammalian cells were inserted into pcDNA3 vectors as described above and transiently expressed using TransIt transfection reagent (Mirus).

Electrophysiology—For S2 cells, cells were seeded on polylysine-coated plates at a confluence of 25% 48–72 h before the experiment. 24–48 h before the experiment cells were transfected, and 500 μM $CuSO_4$ final concentration was added to the medium to induce expression of the channels. For HEK cells, cells were seeded on polylysine-coated plates at a confluence of 25%. 24–48 h before the experiment cells were transfected to induce expression of the channels. Whole-cell currents were recorded at room temperature using borosilicate patch pipettes of 5–8 megaohms and an Axopatch 1D (Molecular Devices) voltage-clamp amplifier. For S2 cells and HEK cells, voltage-clamp pulses in the whole cell configuration using voltage ramps from −140 to 140 mV in 1 s were generated, and data were captured using a Digidata 1322A interfaced to a computer running the pClamp 9.2 software (Axon Instruments). Currents were filtered using the 8-pole low pass Bessel filter of the patch clamp amplifier at 5 kHz and sampled at 50 kHz.

Solutions—For S2 cells, the extracellular Tyrode solution contained 150 mM NaCl, 5 mM KCl, 4 mM $MgCl_2$, 10 mM TES, 25 mM proline, 5 mM alanine, which provided a nominal Ca^{2+}-free solution (0 Ca^{2+}) to which EGTA was added at 0.5 mM or different concentrations of Ca^{2+}. The intracellular solution contained 130 mM potassium gluconate, 10 mM TES, 2 mM $MgCl_2$, 4 mM Mg-ATP, and 0.4 mM Na-GTP. All solutions were titrated to pH 7.15.

For HEK cells the extracellular Tyrode solution contained 137 mM NaCl, 5 mM KCl, 1 mM $MgCl_2$, 1.5 mM $CaCl_2$, 10 mM HEPES, and 10 mM glucose titrated to pH 7.4. The intracellular solution contained 135 mM CsCl, 8 mM NaCl, 5 mM EGTA, 10 mM HEPES and 2 mM Na_2ATP and titrated to pH 7.2. Cells were perfused via BPS-8 valve control system (Scientific Instruments) at a rate of ~30 chamber volumes per minute. Chemicals were applied via the perfusion system. NMDG extracellular solutions contained NMDG replacing NaCl. Linoleic acid (LA) was added to the extracellular solution at a final concentration of 60 μM. Low pH extracellular solution (pH 6.0) contained MES instead of TES and HEPES for experiments in S2 and HEK cells, respectively.

Confocal Imaging—Images of S2 or HEK cells, expressing fluorescent protein-tagged channels, were acquired in a confocal microscope (Olympus Fluoview 300 IX70) using an Olympus UplanF1 60×/0.9 water objective. The cells were excited with argon laser 488 and 568 depending on the fluorescent protein analyzed.

Annexin V Staining—HeLa cells were grown on coverslips and transfected with fluorescent protein constructs. 18 h post-transfection, Alexa Fluor 647 annexin V (BioLegend) was diluted in binding buffer (BioLegend) and incubated with transfected cells for 15 min at room temperature in the dark. After incubation with annexin V, the cells were washed quickly with binding buffer and then fixed in the dark in 4% formaldehyde for 30 min at room temperature. After 3 washes with 1% NH_4Cl (in phosphate-buffered saline), coverslips were then mounted onto glass slides with Antifade Solution (Vysis), and fluorescent images of Alexa Fluor 647 annexin V staining together with fluorescent protein emission were acquired in a confocal microscope (Olympus Fluoview 300 IX70).

Surface Biotinylation Assay—Cell surface proteins were biotinylated and isolated from transfected HEK cells as previously described (47). During this procedure cell lysates were normalized just before isolation of biotinylated cell surface proteins, and after isolation total lysate and cell surface proteins were then probed by immunoblot using the rabbit polyclonal anti-DsRed (Clontech) antibody (which also detects the tdTomato fluorescent protein). The mouse monoclonal anti-glyceraldehyde-3-phosphate dehydrogenase antibody (6C5; Santa Cruz) was used for loading control.

Data Analysis—Data were analyzed and plotted using pClamp 9.2 software (Molecular Devices) and Sigma Plot 8.02 software (Systat software). Confocal images were imported as tiff single images into Photoshop (Adobe Systems Inc.) where they were subsequently cropped and resized.

Statistical Analysis—For statistical analysis Student's *t* test or paired *t* test was used. All error bars are S.E.

RESULTS

The Use of Schneider 2 Drosophila Cells (S2) for Heterologous Functional Expression of Channel Proteins—It was previously found that the *Drosophila* light-sensitive TRPL channels, which are closed in the dark in native tissue, become constitutively active when expressed heterologously in S2 cells (Refs. 44 and 45 and supplemental Fig. 1). In HEK cells only a small leak current was observed at the voltage range of −150 to +150 mV (supplemental Fig. 1*A*). In contrast, in S2 cells, a typical (44, 45) outwardly rectifying I-V curve of TRPL origin was observed (supplemental Fig. 1*B*). As a positive control, we applied LA,

which is known to activate the TRPL channel (44), and an outwardly rectifying I-V curve was observed in HEK cells, whereas enhancement of the TRPL-dependent current was observed in S2 cells (supplemental Fig. 1). These results, thus, demonstrate and confirm our previous observation that TRPL channels become constitutively active when expressed in S2 cells, due to a still unknown reason, and that this system can be utilized for the functional expression of other channel proteins.

To identify a TRPML2-dependent current after heterologous expression of this channel in S2 cells, it was important to distinguish between the putative TRPML2 current and the endogenous S2 current. We found that S2 endogenous currents are relatively small and many times nonexistent (supplemental Fig. 2*A*). When the endogenous current is detected, it shows a distinct inward rectifying I-V curve, which saturates at negative membrane potentials < -100 mV (supplemental Fig. 2*B*) with a negative reversal potential (-55.2 mV $\pm$ 2.9, $n = 16$). Many S2 cells show only a leak current that is not affected by application of LA and has a linear I-V curve of negligible current amplitude (supplemental Fig. 2*A*). On the other hand, when the endogenous S2 current is observed, it is significantly inhibited by application of LA (data not shown).

We observed that S2 cells express mammalian proteins with low efficiency.[3] Therefore, to detect putative functional expression of h-TRPML2 in S2 cells, we tagged the TRPML channel with a fluorescent protein at its C terminus using either YFP or tdTomato conjugates. A previous report showed that C-terminal tagging of h-TRPML2 does not affect the proper subcellular trafficking of the protein (10). Nevertheless, because most of the present study on functional expression of TRPML2 was conducted with tdTomato tagging (48), it was important to show that the tag itself does not affect the channel properties (*i.e.* subcellular distribution and channel activity). The results show that expression of the tdTomato tag alone in S2 cells has no effect upon the endogenous S2 cell I-V curve in control solution or upon application of LA or NMDG (supplemental Fig. 2*C*), whereas its subcellular distribution is of a homogeneously diffuse nature (supplemental Fig. 2*D*), similar to that of the inert green fluorescent protein tag when expressed in many different cell types. This subcellular distribution is markedly different from the distribution seen when tagging h-TRPML2 (see below). Comparing functional expression of h-TRPML2 when tagged with tdTomato or YFP in S2 cells shows that these two tags display negligible effects upon the observed I-V curves (see below). Thus, in aggregate, we conclude that S2 cells are a suitable expression system for mammalian channels even at low expression levels.

Functional Expression of h-TRPML2 in S2 Cells—The h-TRPML2 channel is a 566-amino acid protein that shares ~60% amino acid sequence homology with TRPML1(49). This channel is the least characterized member of the TRPML subfamily. Previous electrophysiological studies have been reported for the TRPML2 channel involving expression of murine TRPML2 mutants (TRPML3-A419P paralogous) in HEK cells. One study, which characterized the longer murine TRPML2-A424P isoform, did not observe any measurable current, leading to the suggestion that TRPML2 might be a nonfunctional channel (28). Another study, which characterized the shorter murine TRPML2-A396P isoform (lacking the first 28 amino acids found in the longer isoform), reported a functional constitutively active channel with the typical inwardly rectifying I-V curve observed in TRPML3-A419P and TRPML1-V432P mutant channels. A third study demonstrated constitutive activity for both the short TRPML2-A396P and the long TRPML2-A424P isoforms with robust inward rectification (21). In addition, the short TRPML2-A396P mutant channel was also found to be iron-permeable and strongly potentiated by low pH (29). Recently, the wild type h-TRPML2 channel was also shown to be active when incorporated into synthetic lipid bilayers (16). Nevertheless, much data describing the characteristics or functional properties of the human or any other wild type TRPML2 channel are yet to be reported. To help fill the gap and especially to compare the properties of wild type (WT) h-TRPML2 with that of h-TRPML2-A424P, we studied the human wild type TRPML2 isoform.

Strikingly, expression of h-TRPML2 in S2 cells revealed a very significant current at negative membrane potentials with an inwardly rectifying I-V curve, similar to I-V curves of other constitutively active TRPML mutant channels (Fig. 1*A*). Very similar I-V curves were obtained with tdTomato or with YFP tagging (Fig. 1*A*), indicating that the fluorescent tag has no effect upon the current. Furthermore, the observed I-V curve was very different from the I-V curve of the endogenous S2 currents with a reversal potential (E_{rev}) of 2.5 $\pm$ 4.09 mV ($n = 10$) and no saturation at negative membrane potentials. Moreover, the functional cell surface expression and vesicular intracellular distribution of h-TRPML2 in S2 cells are consistent with the subcellular distribution of this protein as observed in other cell types as well (10, 15) (Fig. 1*B*). Interestingly, expression of h-TRPML2-YFP or h-TRPML2-tdTomato in HEK cells resulted only in a leak current (Fig. 1*C*) despite the fact that WT h-TRPML2 reaches the cell surface (see below and Fig. 7*D*), whereas expression of h-TRPML2-A424P-tdTomato (Fig. 1*D*) gave a large inward rectifying cationic current (Fig. 1*E*) that also showed permeability to Ca^{2+} (Fig. 1*E*, *top*, *inset*), similar to other paralogous TRPML mutant channels (28).

Taken together, Fig. 1 shows functional expression of h-TRPML2. Importantly, the I-V curve of the WT channel reveals inward rectification similar to that observed from the h-TRPML2-A424P mutant, supporting the notion that the A424P mutation affects the channel open probability by locking the channel in its active state. Nevertheless, we cannot rule out the possibility that the inherent properties of the h-TRPML2 channel (*i.e.* ionic permeability) are altered by introduction of the A424P mutation in a similar manner to the alteration of the A419P mutation upon wild type inherent properties of h-TRPML3 (41).

TRPML2 Channels Are Not Regulated by Ca^{2+} or LA—Many channel proteins are tightly regulated by Ca^{2+} via an open channel block. Experimental evidence has suggested that several members of the TRP family (*e.g.* TRPC2 (50), TRPC6 (51), TRPV3 (52), TRPM6 (53), TRPM7 (54) and the *Drosophila* TRP and TRPL channels (45)) undergo open channel block by diva-

[3] S. Lev and B. Minke, unpublished observations.

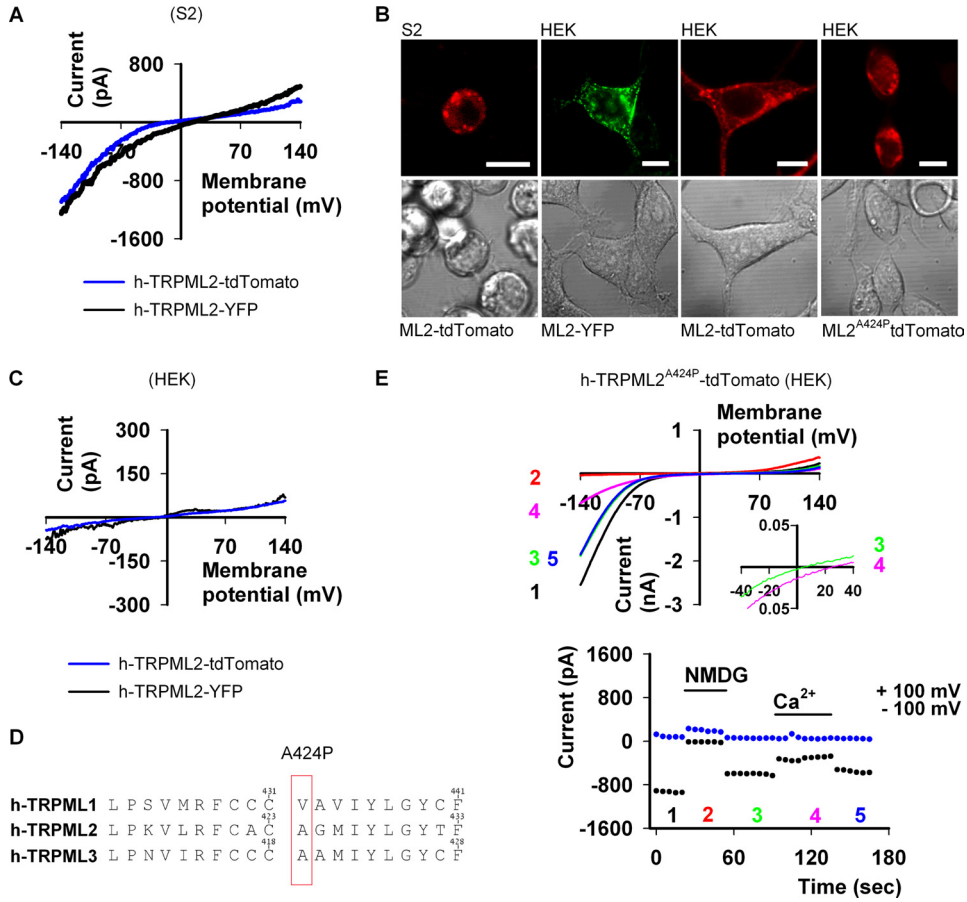

FIGURE 1. **Functional expression of h-TRPML2 in S2 and HEK cells.** *A*, shown are representative I-V curves of h-TRPML2-tdTomato and h-TRPML2-YFP measured from S2 cells by whole-cell patch clamp recordings (Tyrode 0 mM Ca^{2+} solution). *B*, shown is a series of confocal images of h-TRPML2-YFP (*ML2-YFP*) and h-TRPML2-tdTomato (*ML2-tdTomato*) in S2 and HEK cells, as indicated. *Scale bar*, 10 μm. *C*, shown are representative I-V curves of h-TRPML2-tdTomato and h-TRPML2-YFP measured from HEK cells by whole-cell patch clamp recordings (Tyrode wash solution). Note the lack of detectable inward rectifying current from these channels in HEK cells. *D*, amino acid sequence alignment of human TRPML1, TRPML2, and TRPML3 shows the position of the Va mutation (denoted *A424P* in h-TRPML2) in each protein. *E*, *top*, shown are representative I-V curves of h-TRPML2-A424P-tdTomato measured from HEK cells by whole-cell patch clamp recordings. A typical inward rectification is observed (*black*, *green*, and *blue* (*blue* and *green* are superimposed)) curves; Tyrode wash solution) and blocked upon NMDG application (*red curve*). *Inset*, although Ca^{2+} permeates the channel, it permeates to a lesser degree than Na^+ (*green curve*), and at 20 mM external Ca^{2+} (*pink curve*), the E_{rev} shifts to a more positive value (*inset*, *green versus pink* curves). *Bottom*, shown are the current values at +100 (*blue dots*) and −100 mV (*black dots*) as a function of time. The numbers correspond to the curves presented in the *top panel*.

lent cations, especially by Ca^{2+}. It has recently been shown that in addition to the known methods of removing open channel block (either by depolarization or by reducing divalent cation concentration), application of LA is also an efficient way to remove open channel block without depolarization while in the presence of divalent cations (55). LA also strongly affects many types of TRP channels in a still unknown manner (*e.g.* TRPV1 and TRPM8 (55)), giving LA importance as a pharmacological tool to be used in TRP channel research. On this basis it was important to examine whether or not Ca^{2+} or LA application might have an effect upon h-TRPML2 channel activity. Fig. 2 shows that neither a moderate increase in external Ca^{2+} concentration (Fig. 2, *A* and *B*) nor application of LA (Fig. 2*C*) affect the I-V curve of the h-TRPML2 channel in any significant manner, thus ruling out the possibility that Ca^{2+} or LA regulate h-TRPML2 activity in any way. These results differ from those of a previous study involving murine TRPML2-A396P, where facilitation of the TRPML2 mutant current was observed upon removal of Ca^{2+}, suggesting that the A396P mutation alters more than just open probability of TRPML2 channels (29). On the other hand, similar to the effect upon murine TRPML2-A396P, we also observed that replacement of external Na^+ with the non-permeable organic cation NMDG, reduced the h-TRPML2-dependent current and shifted E_{rev} to a negative range typical for the endogenous S2 channels (Fig. 2*D*). These observations, including the fact that h-TRPML2 has a reversal potential close to zero in control solution, indicate that h-TRPML2 is a non-selective cation channel like the murine TRPML2-A396P.

Insertion of Pathology-inducing Mutations Derived from TRPML1 and TRPML3 into the TRPML2 Channel—The TRPML2 channel has not been studied in great detail, probably because this channel has not been associated with any disorder in either humans or in animal models to date. However, the lack of pathological phenotypes may arise from the possibility that mutations in TRPML2 might be embryonic lethal. As all three TRPML channels belong to the same subfamily of TRP channels and share high amino acid sequence homology, it is of utmost importance and physiologically relevant to examine whether mutations in one channel type can induce the same phenotype in other channels because conservation of channel structure and function within a particular channel subgroup. This is certainly the case for the A419P (Va) gain-of-function mutation in TRPML3, whose homologous variant in TRPML1 gives a sustained inward rectifying current otherwise not seen under standard assay conditions (28, 36). This is also true for the murine variants of TRPML2 (21, 29) in addition to the human TRPML2 channel (see Fig. 1*E*).

Various loss-of-function mutations in the TRPML1 protein have been described, most of which have been implicated in MLIV pathogenesis (23, 24). Because of the constitutive activity of h-TRPML2 expressed in S2 cells, it is possible to examine the effect of TRPML1 loss-of-function mutations on the constitutive activity of h-TRPML2.

The F465L missense mutation in the putative ion channel pore region of TRPML1 has been described in MLIV patients with severe disease phenotypes. Although the mutation does not affect the lysosomal subcellular localization of the protein

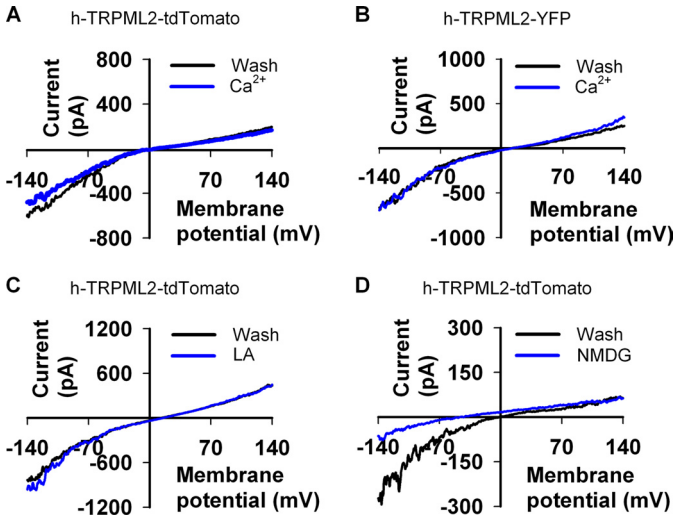

FIGURE 2. **h-TRPML2 is not regulated by Ca^{2+} or LA.** *A*, representative I-V curves measured from S2 cells expressing h-TRPML2-tdTomato (*Wash*, Tyrode 0 mM Ca^{2+} solution; *Ca^{2+}*, Tyrode 5 mM Ca^{2+} solution). The curves show no Ca^{2+} dependence or effect on the channel. *B*, the same I-V curve and lack of Ca^{2+} dependence is seen also for h-TRPML2-YFP expressed in S2 cells. *C* is the same as *A*, showing that LA (60 μM) has no effect on h-TRPML2-tdTomato current. *D* is the same as *A*, showing that h-TRPML2 is a nonspecific cation channel that is blocked by the impermeable organic cation, NMDG.

(12, 30), diminished channel activity has been observed in TRPML1 expression constructs bearing this mutation (29, 56). Amino acid sequence alignment of the putative pore region of TRPML1 with that of the other TRPMLs reveals that the Phe-465 residue in TRPML1 is conserved (Fig. 3*A*, *top*). Therefore, we examined whether the corresponding F457L mutation in h-TRPML2 would lead to a similar reduction of channel activity. Interestingly, we did not observe any significantly smaller current amplitude in S2 cells expressing TRPML2-F457L (Fig. 3*B*). However, unlike h-TRPML2, in which ~80% of the cells marked with tdTomato (and, hence, positive for TRPML2 expression) showed a typical inwardly rectifying I-V curve, less than half of TRPML2-F457L-expressing cells displayed the typical TRPML2 I-V curve (Fig. 3*C*). This could indicate that the mutant channel *per se* is functional, but some mechanism involving protein regulation could be impaired, although the cellular distribution of this mutated channel seems to be normal (Fig. 3*D*).

Within the putative pore region of all three TRPML channels, studies have identified two aspartate residues that lead to impaired cellular phenotypes when mutated to lysine residues. In TRPML1, the D471K/D472K mutant traffics properly to lysosomes like the wild type protein, but unlike the wild type protein, it cannot rescue the transport of lactosylceramide from lysosomes to the Golgi in MLIV patient cells (30). In h-TRPML2, the corresponding D463K/D464K mutant (TRPML2-KK) (Fig. 3*A*, *top*) was reported to display a dominant-negative inhibitory effect upon the recycling of the internalized glycosylphosphatidylinositol-anchored protein, CD59, to the plasma membrane (10). In TRPML3, the corresponding D458K/D459K mutant (TRPML3-KK) (Fig. 3*A*, *top*) was reported to enhance endocytosis of epidermal growth factor receptor while also displaying a dominant-negative inhibitory effect upon starvation-induced autophagy (11). All three of these mutants are predicted to display impaired pore selectivity based on sequence comparisons with other TRPs and the voltage-gated Ca^{2+} channel α-subunit ((CACNLIA1) (30)). However, to date the predicted altered channel activity has not been demonstrated for this mutation in TRPML2 in electrophysiological assays. In Fig. 3 we examined the effect of the D463K/D464K mutation on the h-TRPML2-dependent current. Fig. 3, *B* and *C*, shows that the D463K/D464K mutation completely blocked the h-TRPML2-dependent current when expressed in S2 cells. This was shown by tdTomato marking, which revealed a similar expression pattern as that of h-TRPML2-tdTomato in S2 cells (Fig. 3*D*).

Thus, we demonstrate that it is possible to block activation of the human TRPML2 channel by introduction of missense mutations to the channel pore region. This also potentially explains the inhibitory effect of h-TRPML2-KK upon the recycling of internalized CD59 to the plasma membrane while also demonstrating the similarity in structural functionality among the TRPML channels. In addition, it should be noted that the corresponding KK mutation in TRPML3 was also shown to inhibit the WT (11) as well as the mutant TRPML3-A419P channel when introduced into the protein in *cis* (28). We have also observed that the KK mutation inhibits h-TRPML2-A424P channel activity when introduced into the protein in *cis* (data not shown). This suggests that the KK mutation locks the TRPML3-A419P and h-TRPML2-A424P channels in an inactive state even though these channels possess mutations that supposedly enhance their open probability (28).

Varitint-waddler mice with a milder phenotype (designated Va^J) express a mutant TRPML3 with a second missense mutation (I362T) in *cis* to the severe Va (A419P) mutation. When expressed alone, the I362T mutation in TRPML3 has been shown to render the channel inactive in HEK cells (20). We observed that h-TRPML2 with the corresponding I367T mutation (Fig. 3*A*, *bottom*) expressed in S2 cells is active (Fig. 3*B*). However, like h-TRPML2-F457L, only about half of the cells expressing the mutant channel were found to be active (Fig. 3*C*). This suggests that mutated h-TRPML2 channels are inherently functional, albeit with potentially altered aspects of cellular regulation. These results collectively indicate similarity in structure and function between the three TRPML channels, supporting the notion that they may share several modes of activation and modulation.

Low Extracellular pH Attenuates the Current of Both Native and Mutant h-TRPML2 Channels—It was previously shown that low extracellular pH (4.6) facilitates murine TRPML2-A396P current (29), whereas a significant decrease in current was observed in murine TRPML3-A419P channels under the same conditions (28). On the other hand, another group reported that low extracellular pH (6.0) completely abolished currents of the WT h-TRPML3 channel while displaying little effect upon h-TRPML3-A419P currents (41).

Given these results regarding pH regulation of different WT and mutant TRPML channels, we asked whether a similar difference might be observed between WT and mutant h-TRPML2 channels. Because h-TRPML2 is known to traffic through acidic endosomal and even lysosomal vesicles (10, 15),

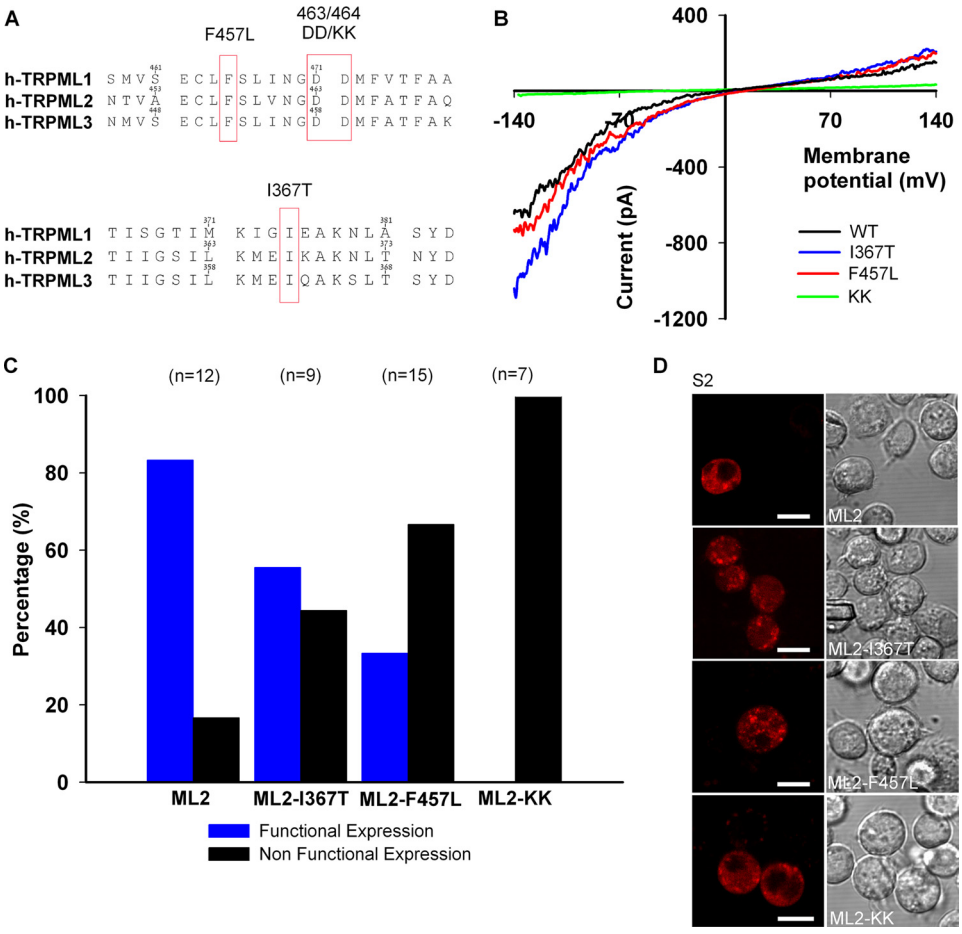

FIGURE 3. **Insertion of pathology inducing mutations derived from TRPML1 and TRPML3 into the TRPML2 channel.** *A*, amino acid sequence alignment of human TRPML1, TRPML2, and TRPML3 shows the position of the denoted h-TRPML2 mutations. *B*, shown are representative I-V curves measured from S2 cells expressing wild type h-TRPML2-tdtomato (WT) and other mutated isoforms (Tyrode 0 mM Ca^{2+} solution). Note that wild type h-TRPML2, h-TRPML2-I367T, and h-TRPML2-F457L I-V curves and current amplitudes are similar. *C*, shown is a histogram presenting the percentage of cells expressing the indicated h-TRPML2-tdTomato channels, which are functional and non-functional, in terms of current amplitude. Note that all h-TRPML2-KK expressing cells are non-functional. *D*, confocal images of S2 cells expressing the indicated h-TRPML2-tdTomato (ML2) isoforms show similar subcellular distribution. *Scale bar*, 10 μm.

the question of extracytosolic pH regulation is of utmost importance when investigating h-TRPML2 cell biological function going forward.

Fig. 4 shows that a reduction of extracellular pH from 7.15 to 6.0 significantly reduces h-TRPML2 current in WT (Fig. 4*A*) as well as I367T (Fig. 4*B*) and F457L (Fig. 4*C*) mutant forms. Moreover, we also observed that this change in negative current amplitude at low extracellular pH is consistently and significantly ~25% lower than that observed when assaying these channels under the physiological extracellular pH of 7.15 (Fig. 4*D*). As expected, low extracellular pH had no effect upon h-TRPML2-KK currents (data not shown), as this channel is inactive. Interestingly, we did not observe any reduction of current from the constitutively active h-TRPML2-A424P mutant in HEK cells in an extracellular pH of 6.0 (Fig. 4*E*). Nevertheless, there was a significant facilitation of the h-TRPML2-A424P current when extracellular pH was further lowered to 4.6 (data not shown), consistent with a previous report describing murine h-TRPML2-A396P under the same conditions (29).

h-TRPML3 Is Constitutively Active in S2 Cells When Expressed in the A419P Mutant Form—Fig. 1*A* shows that in S2 cells, the h-TRPML2 channel is constitutively active. However, in HEK cells, we have shown that h-TRPML2 displays constitutive activity only when possessing the A424P mutation (Fig. 1*E*). In an effort to further characterize human TRPML2 functional properties in S2 cells, we examined the activity of h-TRPML2-A424P. Unfortunately, we were unable to express the A424P (TRPML3 Va mutant paralogue) or A424P+I367T (TRPML3 Va_j mutant paralogue) h-TRPML2 mutants in S2 cells due to inexplicable construct toxicity.

Although it is possible to activate WT TRPML3 by incubating cells in Na^+-free extracellular solution, it has also been demonstrated that TRPML3 is not constitutively active in HEK cells under normal conditions (20, 28, 36). Similarly, we also observed that WT h-TRPML2 does not display constitutive activity in HEK cells under the same conditions (Fig. 1*C*). In S2 cells, however, we have seen that WT h-TRPML2 is constitutively active in Tyrode solution (Fig. 1*A*). This is not the case with WT h-TRPML3 in S2 cells under the same conditions (data not shown). Nevertheless, once we introduced the A419P (Va) mutation into the h-TRPML3 channel, we observed constitutively active and robust currents with a typical inward rectifying I-V curve in our S2 cells (Fig. 5*A*). Moreover, these same features were observed for h-TRPML3-A419P in HEK cells as well (Fig. 5*B*). It should also be noted that the overall cell surface and vesicular intracellular distribution pattern of h-TRPML3-A419P in both S2 and HEK expression systems (Fig. 5*C*) is consistent with previous reports describing TRPML3 subcellular localization in other cell systems (11, 13, 15).

Thus, in contrast to h-TRPML2, we have found that h-TRPML3 is not constitutively active in Tyrode solution in S2 cells unless expressed in its constitutively active A419P mutant form. These results also further qualify S2 cells as a pertinent expression system for characterizing TRPML channels.

Constitutive Activity of TRPML2 and TRPML3 Channels Results in Cellular Degeneration—It has been well established that constitutive activity of TRPML3-A419P causes cellular degeneration, which is attributed to Ca^{2+} overload (20, 28, 37, 38). To examine whether the constitutive activity of the h-TRPML2 channel expressed in S2 cells leads to the same phe-

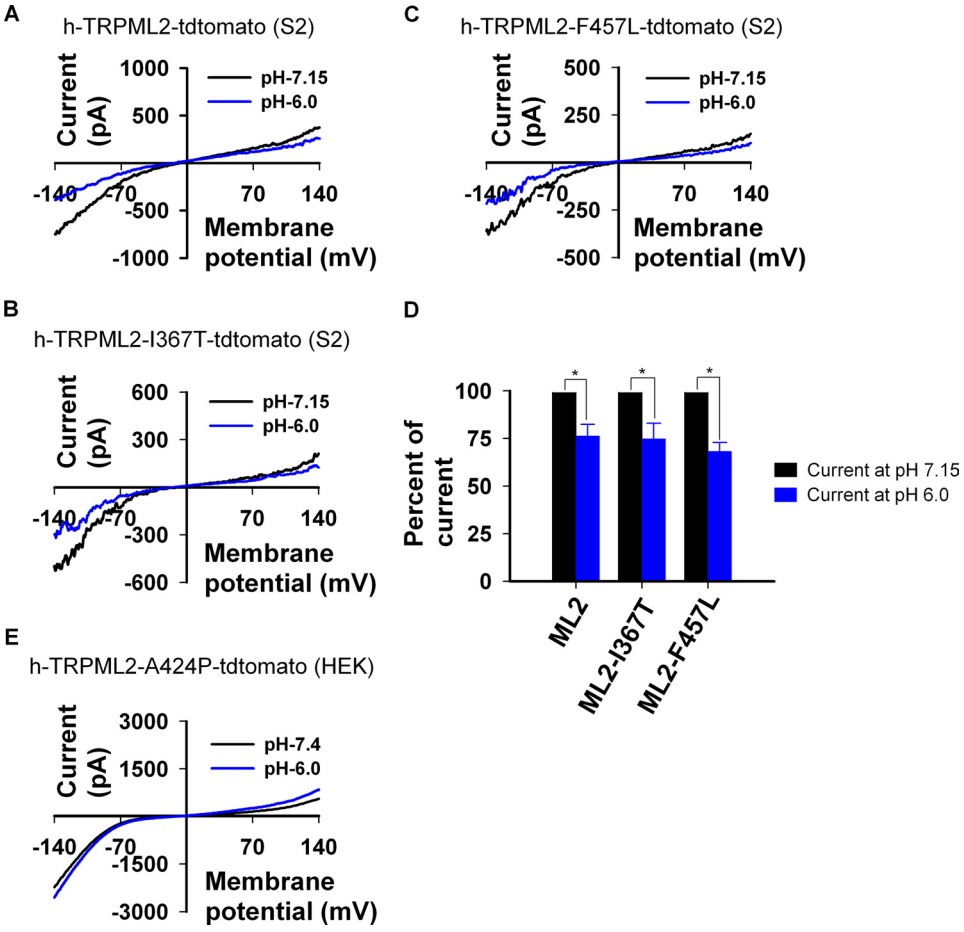

FIGURE 4. **Low extracellular pH reduces the inward current in native and mutant isoforms of h-TRPML2 expressed in S2 cells.** *A*, shown are representative I-V curves measured from S2 cells expressing wild type h-TRPML2-tdTomato in the indicated pH of extracellular solution. Note that lowering of extracellular pH from 7.15 to a value of 6.0 reduces current amplitude significantly. *B* is same experiment as in *A*, with the h-TRPML2-I367T-tdTomato construct. *C* is the same experiment as in *A*, with the h-TRPML2-F457L-tdTomato construct. *D*, shown is a histogram summarizing *A–C* displaying the normalized inward current of the indicated channels at extracellular pH 6.0 relative to their currents at extracellular pH 7.15. Note that the mean reduction of current is the same for all constructs. *E*, representative I-V curves measured from HEK cells expressing h-TRPML2-A424P-tdTomato in the indicated pH of extracellular solution are shown.

notype, we examined the morphology of S2 cells expressing the h-TRPML2 channel. The morphology of degenerated cells was characterized by swelling, total deterioration (loss of morphology), and cell detachment from the glass. Fig. 6, *A* and *B*, shows that 54.5 ± 3.1% of S2 cells expressing the active h-TRPML2 channel, as opposed to 28.8 ± 3.5% of S2 cells expressing the inactive h-TRPML2-KK mutant, present with cell degeneration morphology. In addition, the degeneration of S2 cells expressing h-TRPML3-A419P was even more pronounced (74.6 ± 3.1%) (Fig. 6, *A* and *B*). We found that the current amplitude of h-TRPML3-A419P is larger than that of h-TRPML2 in S2 cells (compare the h-TRPML2 trace in Fig. 3*B* to the h-TRPML3-A419P trace in Fig. 5*A*). This suggests that the extent of cell degeneration in S2 cells corresponds with the magnitude of current that is found upon heterologous expression of h-TRPML2 or h-TRPML3 channels.

To corroborate our findings, we further characterized the morphology of HEK cells expressing either h-TRPML2 or h-TRPML3 channels. We found that expression of WT h-TRPML2 in HEK cells did not lead to any significant cell degeneration (Fig. 6, *C* and *D*), consistent with our observation that the channel is not constitutively active in this expression system (Fig. 1*C*). Similarly, insignificant cell degeneration was also observed in HEK cells expressing WT h-TRPML3 (Fig. 6, *C* and *D*). In contrast, both the constitutively active h-TRPML2 A424P and h-TRPML3-A419P mutant channels induced robust cell degeneration when expressed in HEK cells (Fig. 6, *C* and *D*). These mutant channels also exhibit a robust, constitutive, inwardly rectifying current when expressed in HEK cells (Figs. 1*E* and 5*B*).

Thus, in aggregate, we show that constitutive activity of h-TRPML2 and h-TRPML3 is toxic in both S2 and HEK cell systems. Furthermore, we also show a clear correlation between current amplitude and the extent of cell degeneration in both cell systems.

Apoptosis in h-TRPML2-A424P-expressing Cells Is Caused by the Ca^{2+} Overload and Can Be Rescued with the Ca^{2+} Extrusion Pump, PMCA2—In a recent study it was confirmed that expression of TRPML3-A419P induces apoptosis by causing intracellular Ca^{2+} overload. TRPML3-A419P expressing cells were rescued by co-transfecting them with the plasma membrane calcium extrusion pump, the plasma membrane calcium ATPase type 2 (PMCA2). In effect, PMCA2 was shown to ameliorate the toxic effects of massive intracellular Ca^{2+} concentrations, caused directly by robust inward rectifying TRPML3-A419P currents, by pumping intracellular Ca^{2+} out of cells without showing any effect upon TRPML3-A419P current density (37). Based on our observation that HEK cells expressing h-TRPML2-A424P feature robust inward rectifying currents that are also Ca^{2+}-permeable (Fig. 1*E*), we hypothesized that a similar cytotoxic model was at play.

To confirm that the cell degeneration we observed in cells expressing constitutively active h-TRPML2 channels was caused by Ca^{2+} overload, we sought to rescue cells expressing the toxic h-TRPML2-A424P construct by co-transfecting them with the Ca^{2+} extrusion pump, PMCA2. Fig. 7*A* shows that co-expression of h-TRPML2-A424P with PMCA2 significantly reduces the appearance of morphologically degenerate cells. In addition, annexin V staining for detection of early apoptotic cells revealed a similar rescue when PMCA2 was co-expressed with h-TRPML2-A424P (Fig. 7*B*). Importantly, we also found that PMCA2 co-expression bears no effect upon the

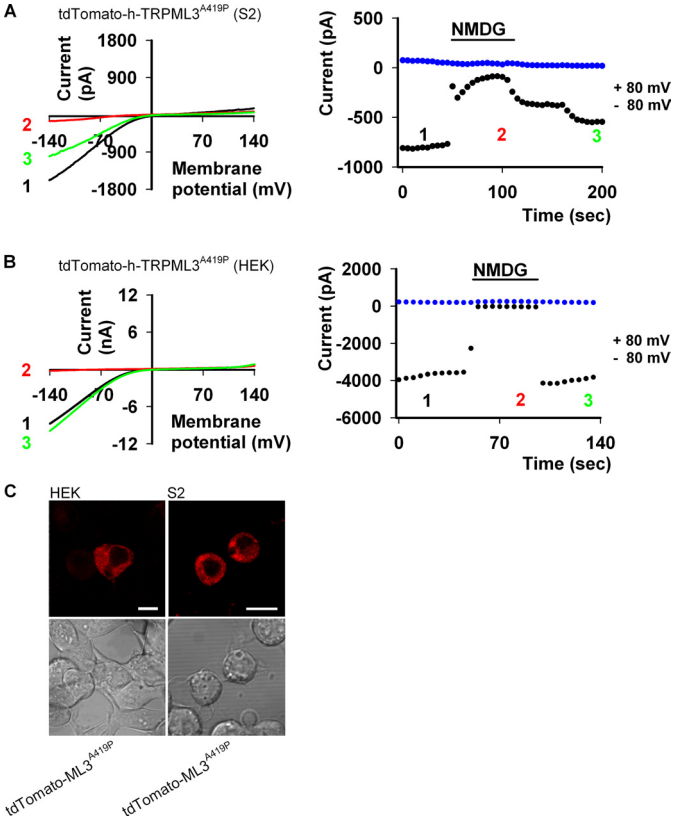

FIGURE 5. **h-TRPML3-A419P is functional and constitutively active in both S2 and HEK cells.** *A*, *left*, shown are representative I-V curves measured from S2 cells expressing tdTomato-h-TRPML3-A419P (*black* and *green curves*; Tyrode 0 mM Ca^{2+} solution) by whole-cell patch clamp recordings. The current is inhibited when Na^+ is replaced by NMDG (*red curve*). *Right*, the current values at +80 (*blue dots*) and −80 (*black dots*) mV are shown as a function of time. The numbers correspond to the curves presented in the *left panel*. *B*, *left*, representative I-V curves measured from HEK cells expressing tdTomato-h-TRPML3-A419P (*black* and *green curves*; Tyrode wash solution) by whole-cell patch clamp recordings. The current is abolished when Na^+ is replaced by NMDG (*red curve*). *Right*, the current values at +80 (*blue dots*) and −80 (*black dots*) mV are shown as a function of time. The *numbers* correspond to the curves presented in the *left panel*. *C*, confocal images are shown of tdTomato-h-TRPML3-A419P in S2 and HEK cells, as indicated. *Scale bar*, 10 μm.

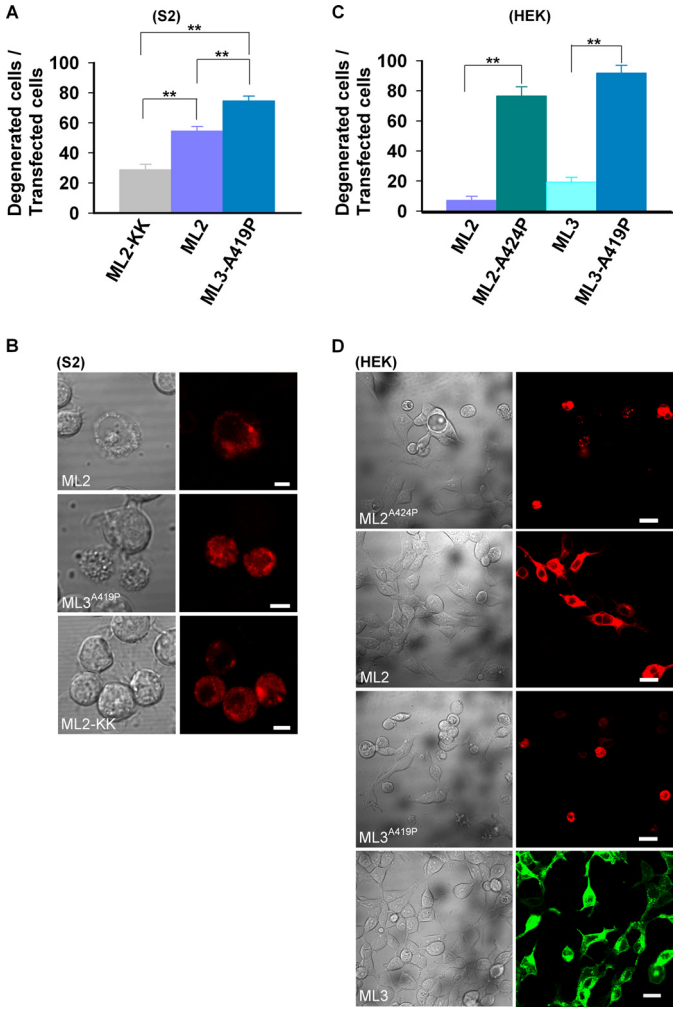

FIGURE 6. **Constitutive activity of both h-TRPML2 and h-TRPML3 results in cellular degeneration.** *A*, shown is a histogram describing the percent of S2 cells expressing the indicated tdTomato-tagged channel types, which also exhibited features of cell degeneration (**, $p < 0.01$). Note a significantly lower cell degeneration in cells expressing the inactive h-TRPML2-KK-tdTomato channel (ML2-KK). *B*, representative confocal images show the extent of degeneration observed in terms of morphological aberrations in S2 cells expressing the indicated tdTomato-tagged channels. Note that normal S2 cell morphology is observed in cells expressing the inactive h-TRPML2-tdTomato-KK channel. *Scale bar*, 5 μm. *C*, shown is a histogram showing the percent of HEK cells expressing EGFP-h-TRPML3 and the indicated tdTomato-tagged channels, which also exhibited features of cell degeneration (**, $p < 0.01$). Note the minimal cell degeneration in cells expressing channels that do not display constitutively active currents in HEK cells (h-TRPML2 (ML2) and h-TRPML3 (ML3)). *D*, representative wide-field confocal images show the extent of degeneration observed in terms of morphological aberrations in HEK cells expressing EGFP-h-TRPML3 and the indicated tdTomato-tagged channels. Note that normal HEK cell morphology is observed in cells expressing h-TRPML2-tdTomato and EGFP-h-TRPML3 channels. *Scale bar*, 20 μm.

h-TRPML2-A424P I-V curve and current amplitude (Fig. 7*C*). Moreover, total and cell surface expression levels of h-TRPML2-A424P are also unaffected by the presence of PMCA2 (Fig. 7*D*). Taken together, these data confirm that apoptosis and cell degeneration of cells expressing constitutively active h-TRPML2 is caused by robust inward rectifying Ca^{2+}-permeable currents that lead to intracellular Ca^{2+} overload.

DISCUSSION

In the present study we were able to functionally express the human wild type TRPML2 channel and describe its electrophysiological properties. *Drosophila* S2 cells assisted us in our analysis by permitting the functional expression of WT h-TRPML2, whereas in other expression systems the same channel exhibited undetectable activity.

New Insights Derived from Functional Expression of WT h-TRPML2—We have seen that constitutive activity of h-TRPML2 leads to cell death. Therefore, we expect that h-TRPML2 channels are carefully regulated under native physiological conditions so as not to enter a constitutively active state. Nevertheless, the ability to express functional, constitutively active h-TRPML2 channels allows for a comparison between the properties of WT h-TRPML2 and mutant h-TRPML2-A424P channels. In this study we observed a striking similarity in current properties between these two isoform channels; both feature an inwardly rectifying I-V curve, and each is a nonselective cation channel, with an E_{rev} close to zero, with no apparent Ca^{2+} regulation, and their constitutive activity leads to cell death. On the other hand, we have observed a discrepancy in terms of pH regulation of these channels. Thus, although it is possible that the A424P mutation locks the chan-

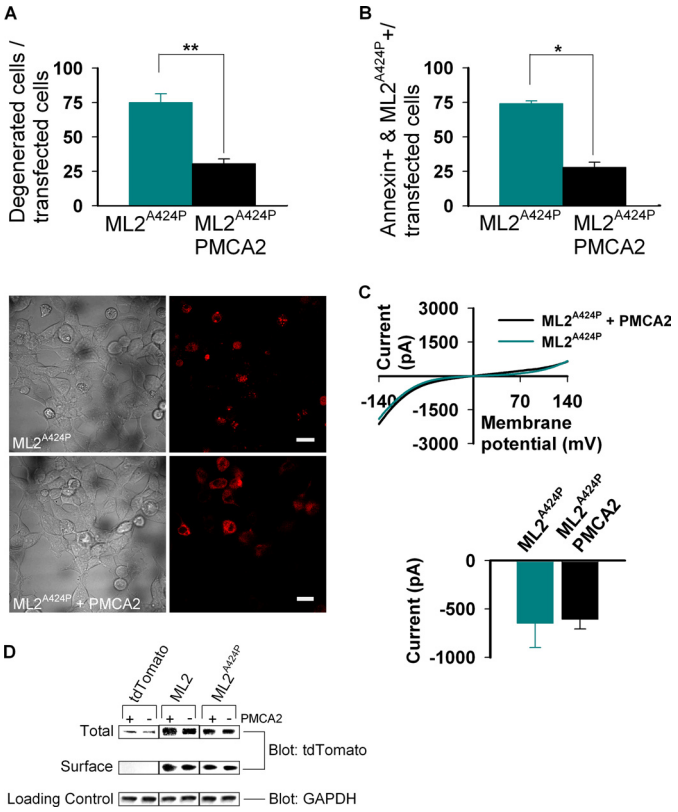

FIGURE 7. **Ca^{2+} induced degeneration caused by constitutive activity of h-TRPML2-A424P is rescued by the calcium pump PMCA2.** *A*, *top*, the histogram shows the percent of degenerated HEK cells after co-transfection of h-TRPML2-A424P (*$ML2^{A424P}$*) with PMCA2 or empty vector (**, $p < 0.01$). Note the rescue of cell degeneration in cells co-transfected with h-TRPML2-A424P and PMCA2. *A, bottom*, wide field confocal images show representative cell morphology in the two groups of co-transfected HEK cells described above (*scale bar*, 20 μm). *B*, shown is a histogram showing the percent of annexin V-positive HeLa cells after co-transfection of h-TRPML2-A424P with PMCA2 or empty vector (*, $p < 0.05$). Note the rescue of cell degeneration in cells co-transfected with h-TRPML2-A424P and PMCA2. *C*, *top*, shown are representative I-V curves of h-TRPML2-A424P in HEK cells after co-transfection with PMCA2 or empty vector. *Bottom*, shown is a histogram of the current amplitude in HEK cells co-transfected with h-TRPML2-A424P and PMCA2 or h-TRPML2-A424P and empty vector. Note that the presence of PMCA2 has no effect on h-TRPML2-A424P-dependent currents. *D*, surface proteins in transfected HEK cells were biotinylated and subsequently isolated from normalized total cell lysates. Pictured are immunoblots of total lysate (*Total*) and surface protein (*Surface*) fractions that were probed for tdTomato-tagged proteins (*Blot: tdTomato*). The endogenous glyceraldehyde-3-phosphate dehydrogenase protein (*Blot: GAPDH*) was probed in total lysates as a loading control (*Loading Control*). Cells were transfected with the tdTomato-tagged constructs, indicated *above each column* of blots in the presence (+) or absence (-) of PMCA2. Transfection of the tdTomato fluorescent protein alone was used as a negative control for the assay. Note that the presence of PMCA2 bears no effect on the total and surface expression levels of both wild type (*ML2*) and mutant (*$ML2^{A424P}$*) h-TRPML2 proteins.

nel in an active state, it might also change inherent properties of the channel.

Regarding the toxicity of constitutively active h-TRPML2, a similar situation was reported for another TRP channel, the *Drosophila* light-activated TRP, which is the founding member of the TRP superfamily (4). The *Drosophila* TRP channel is closed in the dark and cannot be activated by changing the membrane voltage. However, under conditions of metabolic stress, the channel is constitutively active in the dark with native properties typically observed during illumination (57). Constitutive activation of the *Drosophila* TRP channel in the dark under physiological conditions was also obtained by inserting the F550I mutation in the pore region of the channel at transmembrane segment 5. This constitutively active channel has conductance properties similar to the wild type channel, and like the A424P mutation in TRPML2 and A419P mutation in TRPML3 channels, it causes rapid cell degeneration (58).

Because of the high amino acid sequence homology among the three TRPMLs (49), mutations that induce an abnormal phenotype in one TRPML channel can be introduced and studied in other TRPML channels. Accordingly, additional insights into the function of the h-TRPML2 channel were derived by studying the TRPML1 mutation, D471K/D472K, in its corresponding h-TRPML2, D463K/D464K form. This mutation induces in h-TRPML2 a dominant-negative inhibitory effect upon the recycling of internalized CD59 to the plasma membrane (10). Our ability to functionally express and, therefore, characterize h-TRPML2 properties allows examination for the first time of the effect of the D463K/D464K mutation directly upon the native channel without need for an activating A424P-like background mutation (29). The observation that the D463K/D464K mutation completely blocks the h-TRPML2-dependent current confirms the notion that activation of the h-TRPML2 channel is required for proper trafficking of CD59 and perhaps other cargo that traffic along with CD59 through the Arf6-associated pathway (10). Furthermore, the fact that other paralogous TRPML mutations, which were studied in h-TRPML2, demonstrated features that are similar to those observed in the TRPML mutant protein of origin lends the idea that all three channels of the TRPML subfamily share similar regulatory features. This implies that there might be redundancy, at least with regard to TRPML channel function, which would allow for channel substitution as a therapeutic strategy in any pathological state caused directly by gain- or loss-of-function of any one of the TRPML proteins. On the other hand, all three endogenous TRPMLs have been shown to reside in differing subcellular compartments with only partial overlap, and the fact that native TRPML2 and TRPML3 do not compensate for the absence of native TRPML1 in MLIV patient cells (15, 21) suggests that the cellular functions of these proteins are non-redundant. Nevertheless, collectively these findings could imply that the native TRPML channels are active independently and in concert with each other, consistent with our observation that all three TRPML channels heteromultimerize in part (15). Further research should concentrate on the biophysical and physiological relevance of such multimerization and how different mutations combined together act and affect a specific TRPML channel activity.

By assaying the effect of extracytosolic pH upon h-TRPML2 and its mutants, we have already begun to better understand the cell biological function of these channels. h-TRPML2 has previously been shown to traffic dynamically from the cell surface to acidic intracellular vesicles and vice versa (10, 15). In this study, we have demonstrated that h-TRPML2 is also a functional cation channel. What remains to be seen, however, is where in the cell h-TRPML2 becomes active? After demonstrating the mild inhibitory effect of low extracytosolic pH upon h-TRPML2 currents in this study, we may already begin to speculate about the h-TRPML2 channel function in intracellu-

lar vesicles. Either the mild inhibitory effect of low extracytosolic pH on h-TRPML2 channel activity implies that the channel is finely regulated in acidic intracellular vesicles to serve a particular physiological function, or it may also be possible that this effect hints to a lacking in the h-TRPML2 channel function in acidic intracellular vesicles. Future experiments should elucidate the physiological relevance of this limited pH regulation upon h-TRPML2.

The Constitutive Activity of TRPML Channels Induces Cellular Degeneration—We found that the constitutive activation of h-TRPML2 induced cellular degeneration in S2 cells despite seemingly low current densities. Interestingly, constitutive activity of the *Drosophila* TRPL channel, expressed in S2 cells, does not cause any detectable degeneration, although the TRPL channel is a Ca^{2+}-permeable nonselective cation channel that is expressed at high levels in these cells (45). The reason to account for this difference between the effect of constitutive activity of h-TRPML2 *versus* TRPL may arise from the existence of an open channel block mechanism in the TRPL channel (45) that probably does not exist in the h-TRPML2 channel. At resting membrane potentials, the constitutively active TRPL channels are virtually closed in the presence of divalent cations, due to open channel block (45). In the h-TRPML2 channel, the inwardly rectifying I-V curve and lack of Ca^{2+} block result in channels that are widely open, leading to cation overload and degeneration. We found that HEK cells expressing h-TRPML2-A424P featured enhanced inward current and a marked susceptibility to cell death. A similar situation exists with regard to the constitutively active TRP F550I *Drosophila* mutant in which the channel constitutive activity overcomes open channel block at resting potentials in the dark, leading to Ca^{2+} overload and degeneration (58).

h-TRPML2 or h-TRPML3 RNAi Knockdown Results in Cell Degeneration—One of the major questions still pending pertains to the role of the TRPML channels in human physiology. Although not clearly and fully understood, TRPML1 has been shown to contribute to lysosome functionality, whereas a loss-of-function or absence of this protein results in severe motor and ophthalmologic deficits, as manifested in MLIV patients (6). However, the physiological roles of h-TRPML2 and h-TRPML3 are not clear.

Knockdown of h-TRPML2 or h-TRPML3 expression in HEK cells has been shown to cause severe cell degeneration in knockdown cells, which also exhibit lysosomal inclusions and mitochondrial fragmentation in electron micrographs (15). This suggests that the presence of both functional h-TRPML2 and h-TRPML3 channels in the human cell are necessary to ensure cell viability. This might also explain why no loss-of-function mutations have been described for these proteins in any human pathology hitherto. Furthermore, the lysosomal inclusions in h-TRPML2/h-TRPML3 knockdown cells imply that h-TRPML2 and h-TRPML3 may share a lysosomal regulatory role with TRPML1, whose absence in MLIV patient cells leads to a lysosomal storage disorder (25). A concerted mechanism can be thought to exist, also based on experiments showing limited co-localization and physical interactions between the different TRPMLs (15). Nevertheless, the limited nature of these interactions suggests that each of the TRPMLs is likely to play a differing role in the endocytic/exocytic pathways that regulate lysosomal integrity. This possibility will be explored further in light of the similar properties that we have observed in this study among the three TRPML channels.

Conclusions—In this paper we demonstrated and described two extreme facets of human h-TRPML2 channel activity; that is, constitutive activity and the absence of activity. Both lead to impaired cellular function. The constitutively active form is toxic and leads to cellular degeneration, whereas the constitutively inactive form was shown by others to disrupt trafficking along the Arf6-regulated pathway. Therefore, we conclude that the physiologically relevant activation state of h-TRPML2 must reside somewhere in between these two extremes, and the regulatory elements, which control h-TRPML2 activity, must be tuned perfectly to render the channel active according to the physiological needs of a cell. Because we have seen that all three TRPMLs share structural similarities and regulatory regions, future research directed toward understanding the regulation of h-TRPML2 is likely to enable study and characterization of other TRPML channels in a more comprehensive manner. This ultimately allows for the development of therapeutically relevant strategies in conditions where one of the TRPML channels does not function properly and will enhance our understanding of cell and, more directly, endosome-lysosome related function.

Acknowledgments—We thank Ben Katz and Maximilian Peters for critical reading of the manuscript.

REFERENCES

1. Venkatachalam, K., and Montell, C. (2007) *Annu. Rev. Biochem.* **76,** 387–417
2. Minke, B. (2006) *Cell Calcium* **40,** 261–275
3. Ramsey, I. S., Delling, M., and Clapham, D. E. (2006) *Annu. Rev. Physiol.* **68,** 619–647
4. Minke, B., Wu, C., and Pak, W. L. (1975) *Nature* **258,** 84–87
5. Bach, G. (2005) *Pflugers Arch.* **451,** 313–317
6. Zeevi, D. A., Frumkin, A., and Bach, G. (2007) *Biochim. Biophys. Acta* **1772,** 851–858
7. Bezzerides, V. J., Ramsey, I. S., Kotecha, S., Greka, A., and Clapham, D. E. (2004) *Nat. Cell Biol.* **6,** 709–720
8. Damann, N., Voets, T., and Nilius, B. (2008) *Curr. Biol.* **18,** R880–R889
9. Venkatachalam, K., Hofmann, T., and Montell, C. (2006) *J. Biol. Chem.* **281,** 17517–17527
10. Karacsonyi, C., Miguel, A. S., and Puertollano, R. (2007) *Traffic.* **8,** 1404–1414
11. Kim, H. J., Soyombo, A. A., Tjon-Kon-Sang, S., So, I., and Muallem, S. (2009) *Traffic* **10,** 1157–1167
12. Manzoni, M., Monti, E., Bresciani, R., Bozzato, A., Barlati, S., Bassi, M. T., and Borsani, G. (2004) *FEBS Lett.* **567,** 219–224
13. Martina, J. A., Lelouvier, B., and Puertollano, R. (2009) *Traffic.* **10,** 1143–1156
14. Vergarajauregui, S., and Puertollano, R. (2006) *Traffic.* **7,** 337–353
15. Zeevi, D. A., Frumkin, A., Offen-Glasner, V., Kogot-Levin, A., and Bach, G. (2009) *J. Pathol.* **219,** 153–162
16. Curcio-Morelli, C., Zhang, P., Venugopal, B., Charles, F. A., Browning, M. F., Cantiello, H. F., and Slaugenhaupt, S. A. (2010) *J. Cell. Physiol.* **222,** 328–335
17. Strübing, C., Krapivinsky, G., Krapivinsky, L., and Clapham, D. E. (2001) *Neuron* **29,** 645–655
18. Zhang, P., Luo, Y., Chasan, B., González-Perrett, S., Montalbetti, N., Timpanaro, G. A., Cantero, Mdel R., Ramos, A. J., Goldmann, W. H., Zhou, J., and Cantiello, H. F. (2009) *Hum. Mol. Genet.* **18,** 1238–1251

19. Schaefer, M. (2005) *Pflugers Arch.* **451,** 35–42
20. Kim, H. J., Li, Q., Tjon-Kon-Sang, S., So, I., Kiselyov, K., and Muallem, S. (2007) *J. Biol. Chem.* **282,** 36138–36142
21. Samie, M. A., Grimm, C., Evans, J. A., Curcio-Morelli, C., Heller, S., Slaugenhaupt, S. A., and Cuajungco, M. P. (2009) *Pflugers Arch.* **459,** 79–91
22. Sun, M., Goldin, E., Stahl, S., Falardeau, J. L., Kennedy, J. C., Acierno, J. S., Jr., Bove, C., Kaneski, C. R., Nagle, J., Bromley, M. C., Colman, M., Schiffmann, R., and Slaugenhaupt, S. A. (2000) *Hum. Mol. Genet.* **9,** 2471–2478
23. Altarescu, G., Sun, M., Moore, D. F., Smith, J. A., Wiggs, E. A., Solomon, B. I., Patronas, N. J., Frei, K. P., Gupta, S., Kaneski, C. R., Quarrell, O. W., Slaugenhaupt, S. A., Goldin, E., and Schiffmann, R. (2002) *Neurology* **59,** 306–313
24. Slaugenhaupt, S. A. (2002) *Curr. Mol. Med.* **2,** 445–450
25. Bach, G. (2001) *Mol. Genet. Metab.* **73,** 197–203
26. Cantiello, H. F., Montalbetti, N., Goldmann, W. H., Raychowdhury, M. K., González-Perrett, S., Timpanaro, G. A., and Chasan, B. (2005) *Pflugers Arch.* **451,** 304–312
27. Raychowdhury, M. K., González-Perrett, S., Montalbetti, N., Timpanaro, G. A., Chasan, B., Goldmann, W. H., Stahl, S., Cooney, A., Goldin, E., and Cantiello, H. F. (2004) *Hum. Mol. Genet.* **13,** 617–627
28. Xu, H., Delling, M., Li, L., Dong, X., and Clapham, D. E. (2007) *Proc. Natl. Acad. Sci. U.S.A.* **104,** 18321–18326
29. Dong, X. P., Cheng, X., Mills, E., Delling, M., Wang, F., Kurz, T., and Xu, H. (2008) *Nature* **455,** 992–996
30. Pryor, P. R., Reimann, F., Gribble, F. M., and Luzio, J. P. (2006) *Traffic.* **7,** 1388–1398
31. Soyombo, A. A., Tjon-Kon-Sang, S., Rbaibi, Y., Bashllari, E., Bisceglia, J., Muallem, S., and Kiselyov, K. (2006) *J. Biol. Chem.* **281,** 7294–7301
32. Zhang, F., Jin, S., Yi, F., and Li, P. L. (2008) *J. Cell Mol. Med.*, Epub ahead of print
33. Lindvall, J. M., Blomberg, K. E., Berglöf, A., Yang, Q., Smith, C. I., and Islam, T. C. (2004) *Eur. J. Immunol.* **34,** 1981–1991
34. Lindvall, J. M., Blomberg, K. E., Wennborg, A., and Smith, C. I. (2005) *Cell. Immunol.* **235,** 46–55
35. Di Palma F., Belyantseva, I. A., Kim, H. J., Vogt, T. F., Kachar, B., and Noben-Trauth, K. (2002) *Proc. Natl. Acad. Sci. U.S.A.* **99,** 14994–14999
36. Grimm, C., Cuajungco, M. P., van Aken, A. F., Schnee, M., Jörs, S., Kros, C. J., Ricci, A. J., and Heller, S. (2007) *Proc. Natl. Acad. Sci. U.S.A.* **104,** 19583–19588
37. Grimm, C., Jörs, S., and Heller, S. (2009) *J. Biol. Chem.* **284,** 13823–13831
38. Nagata, K., Zheng, L., Madathany, T., Castiglioni, A. J., Bartles, J. R., and García-Añoveros, J. (2008) *Proc. Natl. Acad. Sci. U.S.A.* **105,** 353–358
39. van Aken, A. F., Atiba-Davies, M., Marcotti, W., Goodyear, R. J., Bryant, J. E., Richardson, G. P., Noben-Trauth, K., and Kros, C. J. (2008) *J. Physiol.* **586,** 5403–5418
40. Cable, J., and Steel, K. P. (1998) *Hear. Res.* **123,** 125–136
41. Kim, H. J., Li, Q., Tjon-Kon-Sang, S., So, I., Kiselyov, K., Soyombo, A. A., and Muallem, S. (2008) *EMBO J.* **27,** 1197–1205
42. Bautista, D. M., Siemens, J., Glazer, J. M., Tsuruda, P. R., Basbaum, A. I., Stucky, C. L., Jordt, S. E., and Julius, D. (2007) *Nature* **448,** 204–208
43. Schneider, I. (1972) *J. Embryol. Exp. Morphol.* **27,** 353–365
44. Chyb, S., Raghu, P., and Hardie, R. C. (1999) *Nature* **397,** 255–259
45. Parnas, M., Katz, B., and Minke, B. (2007) *J. Gen. Physiol.* **129,** 17–28
46. Ho, S. N., Hunt, H. D., Horton, R. M., Pullen, J. K., and Pease, L. R. (1989) *Gene* **77,** 51–59
47. Dong, X. P., Wang, X., Shen, D., Chen, S., Liu, M., Wang, Y., Mills, E., Cheng, X., Delling, M., and Xu, H. (2009) *J. Biol. Chem.* **284,** 32040–32052
48. Shaner, N. C., Campbell, R. E., Steinbach, P. A., Giepmans, B. N., Palmer, A. E., and Tsien, R. Y. (2004) *Nat. Biotechnol.* **22,** 1567–1572
49. Puertollano, R., and Kiselyov, K. (2009) *Am. J. Physiol. Renal Physiol.* **296,** F1245–F1254
50. Lucas, P., Ukhanov, K., Leinders-Zufall, T., and Zufall, F. (2003) *Neuron* **40,** 551–561
51. Spassova, M. A., Hewavitharana, T., Xu, W., Soboloff, J., and Gill, D. L. (2006) *Proc. Natl. Acad. Sci. U.S.A.* **103,** 16586–16591
52. Hu, H. Z., Xiao, R., Wang, C., Gao, N., Colton, C. K., Wood, J. D., and Zhu, M. X. (2006) *J. Cell. Physiol.* **208,** 201–212
53. Topala, C. N., Groenestege, W. T., Thébault, S., van den Berg, D., Nilius, B., Hoenderop, J. G., and Bindels, R. J. (2007) *Cell Calcium* **41,** 513–523
54. Nadler, M. J., Hermosura, M. C., Inabe, K., Perraud, A. L., Zhu, Q., Stokes, A. J., Kurosaki, T., Kinet, J. P., Penner, R., Scharenberg, A. M., and Fleig, A. (2001) *Nature* **411,** 590–595
55. Parnas, M., Katz, B., Lev, S., Tzarfaty, V., Dadon, D., Gordon-Shaag, A., Metzner, H., Yaka, R., and Minke, B. (2009) *J. Neurosci.* **29,** 2371–2383
56. Kiselyov, K., Chen, J., Rbaibi, Y., Oberdick, D., Tjon-Kon-Sang, S., Shcheynikov, N., Muallem, S., and Soyombo, A. (2005) *J. Biol. Chem.* **280,** 43218–43223
57. Agam, K., von Campenhausen, M., Levy, S., Ben-Ami, H. C., Cook, B., Kirschfeld, K., and Minke, B. (2000) *J. Neurosci.* **20,** 5748–5755
58. Yoon, J., Ben-Ami, H. C., Hong, Y. S., Park, S., Strong, L. L., Bowman, J., Geng, C., Baek, K., Minke, B., and Pak, W. L. (2000) *J. Neurosci.* **20,** 649–659